Journal of Alloys and Compounds 969 (2023) 172343

Contents lists available at ScienceDirect

Journal of Alloys and Compounds

journal homepage: www.elsevier.com/locate/jalcom

Research Article

Oxidation protection of TNM alloys with Al-rich γ-TiAl-based coatings

S. Kagerer [a], O.E. Hudak [a,b], T. Wojcik [a,b], R. Hahn [b], A. Davydok [c], M. Schloffer [d], H. Riedl [a,b], P. H. Mayrhofer [a,*]

[a] Institute of Materials Science and Technology, TU Wien, A-1060 Wien, Austria
[b] Christian Doppler Laboratory for Surface Engineering of high-performance Components, TU Wien, Austria
[c] Helmholtz-Zentrum Hereon, Institut für Werkstoffphysik, Notkestr 85 22607, Hamburg, Germany,
[d] MTU Aero Engines AG, D-80995 Muenchen, Germany

ARTICLE INFO

Keywords:
Oxidation resistance
TNM
PVD coatings
HR-TEM
Nano beam diffraction
T-EBSD

ABSTRACT

The request to reduce carbon emissions as well as fuel consumptions of modern aerospace and aviation mobility, heavily motivated the development of lighter and more durable high temperature materials. γ-TiAl bulk materials meet many of these requirements due to their unique properties, such as low density, high strength or excellent creep resistance. However, improving their oxidation resistance above 750 °C is still challenging, especially without deteriorating other material properties. Recently, we showed that magnetron sputtered Al-rich γ-TiAl coatings are ideal candidates for well-established TNM bulk alloys (Ti-43.5Al-4Nb-1Mo-0.1B, in at%) to increase their oxidation resistance and to block oxygen inward diffusion. Within this study, we present detailed microstructural investigations of the appearing phase transformations and morphological changes in the coating due to ambient-air-exposure at 850 °C for up to 1000 h. These show that only a 4-μm-thin, well-adhering α-Al_2O_3-based thermally grown oxide (TGO) forms on top of an initial 16.5-μm-thick coating. Cross-sectional nanobeam diffraction in conjunction with high resolution chemical as well as structural analysis during transmission electron microscopy after these exposures highlight that the Al-rich γ-TiAl coating is perfectly intermixed with the TNM substrate material. Already after 100 h oxidation at 850 °C, no interface between the Al-rich γ-TiAl coating and the TNM alloy can be identified chemically or structurally. The structural homogenization is governed by the transformation of all Al-rich phases (i.e., $TiAl_3$ or Ti_2Al_5) – also present in the as-deposited state – towards γ-TiAl. After 1000 h at 850 °C, the predominant phase within the original coating region is γ-TiAl, next to the highly dense and well-adherent α-Al_2O_3-based scale.

1. Introduction

Titanium aluminides, especially intermetallic γ-TiAl alloys have gained a lot of attention as lightweight high temperature material in industry and science. The excellent creep resistance combined with outstanding mechanical properties are comparable with Ni-based super alloys [1–3], but with a significantly lower density (of 3.9–4.2 g/cm^3). Up to 750 °C, industrial established TiAl alloys, such as the so-called TNM (Ti-43.5Al-4Nb-1Mo-0.1B, with element composition in at%), provide an appropriate oxidation resistance. This originates from a thin mixed TiO_2 and Al_2O_3-based oxide scale. Above this temperature, the fast growing and under-dense TiO_2 formation leads to non-protective scales [4]. These thermally grown oxides (TGO) typically lead to spallation, which promotes break-through oxidation [4,5]. Higher Al-contents could promote the formation of denser Al_2O_3-based scales even above 750 °C, but with the drawback of significant reduction in strength and ductility – caused by the presence of $TiAl_2$ and $TiAl_3$-based phases [2,6,7].

There are different approaches to increase the oxidation resistance of γ-TiAl alloys beyond 750 °C, such as promoting the alumina formation due to chlorine or fluorine treatments (using the so-called halogen effect). However, such treatments typically influence the mechanical properties of the used alloys [8–10]. An alternative way is the plasma assisted deposition of Al-rich γ-TiAl-based coatings on top of the TNM alloy. Through the chemical resemblance of the coating and bulk material, excellent adhesion and oxidation properties can be achieved [11]. Thermal barrier coatings can further increase the service temperature by reducing the thermal impact onto the TNM alloy, respectively Al-rich γ-TiAl-based coating [12]. In general, physical vapor deposition (PVD) with its low deposition temperatures offers a wide range of possibilities

* Correspondence to: Materials Science and Technology, TU Wien, Getreidemarkt 9, A-1060 Wien, Austria.
E-mail address: paul.mayrhofer@tuwien.ac.at (P.H. Mayrhofer).

https://doi.org/10.1016/j.jallcom.2023.172343
Received 21 December 2022; Received in revised form 8 September 2023; Accepted 26 September 2023
Available online 28 September 2023

to prepare protective coatings and diffusion barriers even on thermally-sensitive materials [13]. Protective coatings are typically ceramic-based materials (like nitrides and oxides) shielding the underlying bulk material against wear or oxidation [14–16]. The different material characteristics between these ceramics and metallic alloys (with their differential thermal expansion coefficients) often lead to delamination, especially during thermal cycling (as present for turbine blade materials). This particular problem can be overcome by using transition layers or preparing metallic diffusion coatings (like an Al-rich γ-TiAl-based coating), providing the ability to form stable oxides such as Al_2O_3, SiO_2, or Cr_2O_3. In addition to the supported formation of such protective oxides, these coating materials diffuse into the surface region of the bulk material forming an essentially perfect transition between protective oxides and bulk. Therefore, such diffusion-driven coating concepts typically have an excellent adhesion to the substrate material (by forming a homogeneous transition zone with a matched thermal expansion coefficient). MCrAlY coatings are well known for their excellent ability to form dense and protective thermally grown oxides (TGO) [17]. Braun et al. [18–20] proved by several studies that the oxidation resistance of γ-TiAl alloys hugely increases when protected with TiAlCr-based coatings. However, Cr diffusion into the TNM alloy leads to unintended microstructural changes, harming the microstructure [18,21].

Implementing all these considerations, we recently showed that Al-rich γ-TiAl-based coatings deposited onto the TNM alloy – the coating has the same Nb and Mo content as the TNM alloy but a higher Al content – allows for the formation of a dense and well-adherent Al_2O_3-based TGO. The Al-rich γ-TiAl-based coating itself forms a perfect transition region with the TNM alloy and serves as an Al-reservoir to support the continuous TGO formation at higher temperatures as well as long-term exposures [11]. Here, we provide further insights to the microstructural evolution of an Al-rich γ-TiAl-based coating upon the ambient-air-exposure at 850 °C by employing high resolution transmission electron microscopy (HR-TEM), transmission-electron backscatter diffraction (t-EBSD), as well as nano beam diffraction.

2. Materials and methods

Al-rich γ-TiAl-based coatings were prepared by unbalanced magnetron sputtering of a 6-inch TiAl-GD7100 target (Ti-62Al-4Nb-1Mo-0.3(B+Y) in at% [22,23]) in Ar-glow discharges using an "in-house" developed system [24]. The sputter-target (bottom-up configuration) was tilted by 20° to the substrate (20° between the normal of substrate and target) and driven by a Solvix HIP^3 5 generator. Heat treated and surface conditioned TNM (Ti-43.5Al-4Nb-1Mo-0.1B) and TiAl-GD7100 substrates (hot isostatic pressed) were mounted on a rotatable 180 mm diameter substrate holder (facing the sputter-targets at a distance of ~147 mm), which was powered by an MKS ENI RPG-50 5 kW generator for Ar-ion etching and biasing during deposition. Prior to loading the substrates to the deposition chamber, they were cleaned with sodium-hydroxide and 2-aminoethanol cleaning solvent. Subsequently, to avoid selective attack, the cleaning solution was removed with distillated water in an ultrasonic bath for 10 min.

All depositions were carried out with a substrate temperature of T_{sub} = 280 °C. Prior to the Ar-ion etching and after the deposition process, the temperature was maintained at least for 20 min. Ar-ion etching of the samples was conducted with a pressure p_{etch} = 6 Pa for 10 min applying a potential of −500 V DC on the rotating substrate holder (v_{rot} = 90 rad/s). The depositions were conducted with an Ar pressure of 0.4 Pa and powering the TiAl-GD7100 sputter-target with 4.5 W/cm^2 and applying a bias potential of −50 V DC to the TNM and TiAl-GD7100 substrates.

The samples with a coating thickness of 16.5 μm in their as-deposited state were oxidized inside a standard chamber furnace at 850 °C in ambient air for 100, 300, 600, and 1000 h (using individual samples from the same deposition run for the different times). To ensure constant temperature conditions, the samples were placed into the furnace at 850 °C, without any pre-heating. After the individual times, the samples were removed and cooled down in ambient air at room temperature. The oxidized samples were hot mounted using a carbon-rich embedding material, to ensure electrical conductivity (needed for the scanning electron microscopy, SEM, investigations) and mechanical support (especially to the oxide formed onto the sample) for the subsequent metallographic cross-sectional sample preparation with a semi-automatic system (Struers Tegra).

The chemical composition of the Al-rich γ-TiAl coatings was obtained by energy-dispersive X-ray spectroscopy (EDS, FEI Philips XL30 with an EDAX EDS detector 20 kV accelerating voltage). Detailed SEM investigations are conducted with a FEI Quanta 200 SEM equipped with a field emission gun and a circular back-scattered electron (BSE) detector. A special transmission Kikuchi diffraction (TKD, or transmission electron backscatter diffraction, t-EBSD) sample holder allows for detailed grain-size, grain-size distribution, and grain orientation analysis.

Samples for transmission electron microscopy (TEM) were cross-sectional prepared using a focused ion beam (FIB, FEI Quanta 200 3D) workstation (Ga^+ ions for milling). To prevent damage during this preparation, the sample surface was coated with a thin Pt-layer. After transferring the FIB-machined sample piece to a TEM grid, it was ion-thinned and polished (starting with an acceleration voltage of 30 kV and a current of 5 nA, which was stepwise reduced to 0.1 nA), all inside the FIB workstation. If necessary, further gentle sample-thinning was done with a Gatan PIPS II in low-voltage-mode to increase TEM transparency. Detailed structural and chemical analysis (EDS) were conducted with a TECNAI F20 FEG TEM (equipped with an EDAX Apollo XLT 2 detector) in bright field TEM and scanning mode (STEM). For structural analysis by selected area electron diffraction (SAED) we used aperture sizes of 650 or 170 nm diameter.

Nano beam diffraction experiments were performed at the nanofocus endstation of beamline P03 – PETRA III at DESY (Hamburg, Germany) [25] – with a monochromatic X-ray radiation having a wavelength of λ = 0.80533 Å (15.4 keV beam energy). The lamella used for these measurements were cut as a cross section (~0.5 mm thickness) from an oxidized sample (using a Struers Accutom equipped with a diamond cutting blade), and subsequently polished on both sides to a final thickness of ~50 μm. Prior to the measurements, a LaB_6 powder standard was measured to obtained the exact sample-detector distance and beam center. The samples were placed in transmission geometry to collect Debye Scherrer patterns using a cross sectional approach, as described in [26]. The beam geometry was set to a size of ~1.5 × 1.5 μm^2 by means of KB mirrors, and the step width for cross sectional scanning was set to 850 nm. The diffraction signal was recorded with a Dectris Eiger 9 M detector with an active area of 57,180.64 mm^2 and 75 × 75 μm^2 pixel size. For the setup-calibration and the full ring integration in azimuthal direction of the collected patterns, the open source tool DPDAK was used [27]. The above-mentioned wavelength was implemented in the diffraction pattern using the ICDD PDF-4 + 2021 software package to evaluate the phases present.

To avoid any edge effects, the samples for XRD and TEM studies were taken far away from the side-edges of the (oxidized) specimens.

3. Results and discussion

Metallic Al-rich coatings allow to form a thermally grown oxide accompanied by an excellent coating-to-substrate (if metallic) adhesion. The outstanding adhesion properties are typically further improved through interdiffusion between coating and substrate. Especially, the Al-rich γ-TiAl-based coatings deposited on a TNM substrate obtain a specific diffusion profile. The initially relatively sharp chemical gradient (immediately after the deposition) is schematically shown in Fig. 1a. This sharp transition from coating to substrate is especially visible in BSE-SEM contrast (Fig. 1a, middle). The featureless (in BSE-contrast)

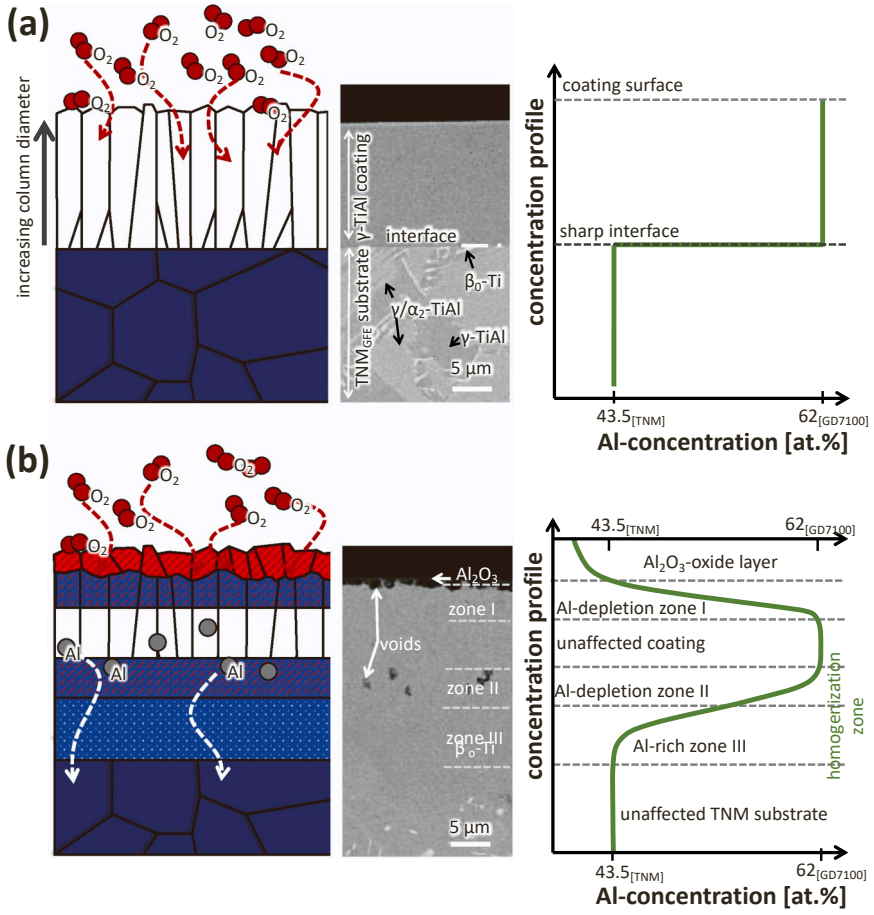

Fig. 1. Schematic figure of cross-sectional morphology as well as Al profile of the γ-TiAl-based coated TNM alloy in its as-deposited state (a) and after 100 h treatment at 850 °C in ambient air (b). The schema is based on cross-section SEM and EDS studies. Exemplarily, the corresponding cross-sectional BSE-SEM images are added to (a) and (b) [11].

coating consists of 50–200 nm wide columnar grains (schematically shown in Fig. 1a, left), with an excellent adhesion to the TNM alloy already in the as-deposited state. This coating, containing 62.0 at% Al, consists of nanocrystalline γ-TiAl grains next to over-stoichiometric Al-rich-based phases such as $TiAl_3$, Ti_2Al_5, or $TiAl_2$ (as proven by XRD, not shown here). The microstructure of the TNM bulk material is characterized through its larger α_2/γ-TiAl grains surrounded by β_0-phases (having an average Al-content of 43.5 at%). After thermal exposure at 850 °C for 100 h, three different zones concerning the Al-content can be identified within the coating and the interface-near region, see the sketch in Fig. 1b. At the surface of the coating a dense Al_2O_3-based TGO is formed, due to which the coating is depleting in Al, indicated as Al-depletion Zone I in Fig. 1b (see also the schematic Al-concentration on the right side). Beneath this zone, the original high Al content of the coating is still present, serving as an Al-reservoir to further support the formation of a dense protective TGO. Because the coating itself has a higher Al content than the TNM alloy, also towards the TNM alloy there is cross-diffusion leading to the formation of another Al-depletion zone in the coating (indicated as Zone II in Fig. 1b, right). Accordingly, within the TNM alloy an Al-rich zone is formed (indicated as Al-enriched Zone III in Fig. 1b, right), which basically does not show anymore the typical TNM microstructure. These zones (Al-depleted Zone II of the coating and Al-enriched Zone III of the TNM alloy) build together the transition zone indicated as homogenization zone and marked as greenish area in Fig. 1b. The regions out of which Zone II and III formed had a sharp interface in the as-deposited state, this cannot be detected anymore due to intermixing by interdiffusion. Below this homogenization zone, the original TNM microstructure is still present.

Detailed TEM-investigations of the as-deposited coating, Fig. 2a, clearly show its dense and columnar growth morphology. The typical competitive growth morphology can easily be recognized especially in Fig. 2b, which also shows part of the TNM substrate. The initial crystal growth during deposition starts with random oriented nuclei leading to initially small grains, which are overgrown by oriented grains leading to the columnar morphology. Although chemically very similar, the interface between the Al-rich TiAl-based coating and the TNM substrate can easily be identified. The EDS line scan across this interface clearly shows their difference in Al content starting at 43 at% Al within the TNM alloy to about 62 at% within the coating (Fig. 2c). TEM-EDS measurements within the TNM substrate are affected by their local presence of larger grains of α, β, and/or γ phases, which have other Al-equilibrium contents than 43.5 at% Al, see the phase diagram, Fig. S1.

The Nb and Mo content within the film is in good agreement to the TiAl-GD7100 sputter-target material (used to prepare the coatings). The slightly increased oxygen signal at the vicinity to the interface between TNM alloy and γ-TiAl-based coating (see green line in Fig. 2c) originates from the native oxide formed on the TNM alloy substrate, which could not fully be removed by the argon ion etching process prior to the deposition. When growing the film on a TiAl-GD7100 substrate, the interface between substrate and coating is still recognizable due to their pronounced microstructural difference (Fig. 2d). The TEM-EDS line scan across the interface shows no difference (Fig. 2e), which confirms that the film is chemically identical to the sputter-target. The direct comparison in chemistry between the TiAl-GD7100 substrate and the film prepared from such a target material, allows to conclude that the sputter deposition process itself (with all the characteristics like different

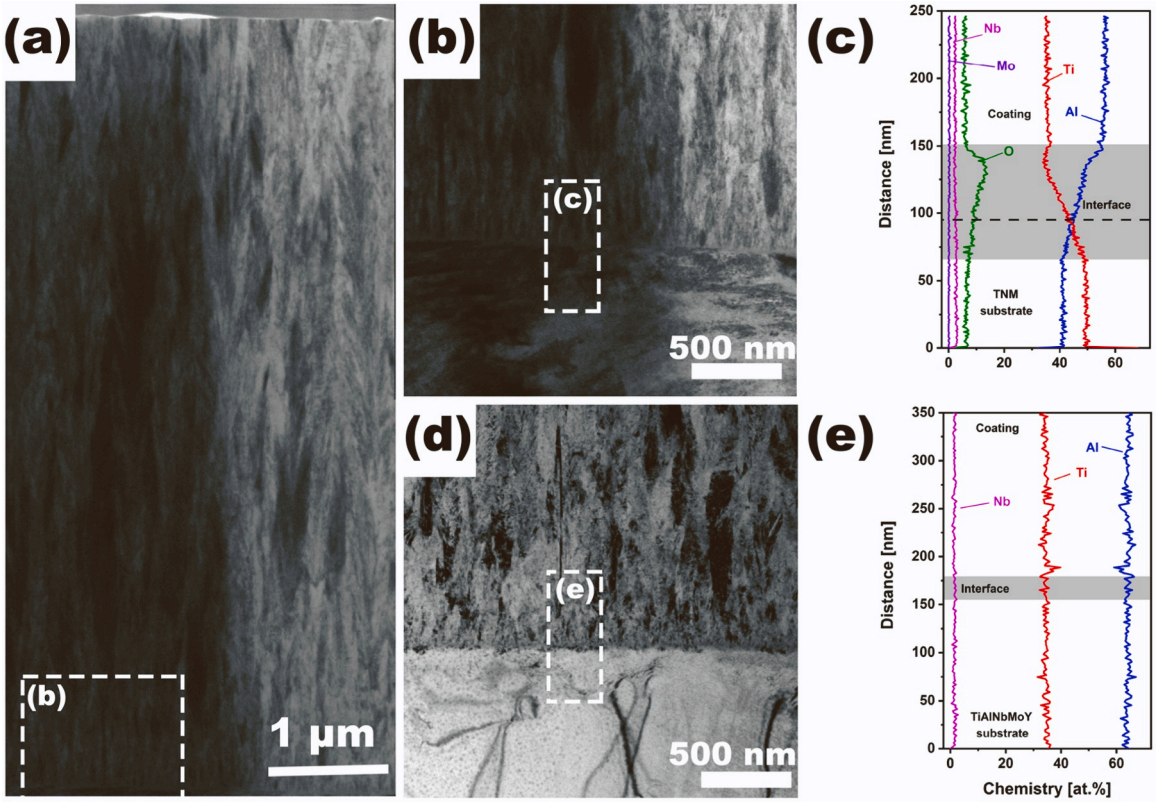

Fig. 2. (a) Cross-sectional TEM bright field image of the γ-TiAl-based coating in the as-deposited state consisting of nanocrystalline γ-TiAl as well as Al-rich-based phases, i.e., $TiAl_3$, Ti_2Al_5, or $TiAl_2$. A detailed depiction of the interface to the TNM alloy (43.5 at% Al) is given in (b), whereas the corresponding interface of this coating deposited on the TiAl-GD7100 (62 at% Al) substrate is shown in (d). The respective EDS line-scans are presented in (c) and (e).

sputter yields of the elements within the target, scattering, and resputtering effects) has no (within the error of the EDS measurements) influence on the chemistry.

The morphological changes investigated by back-scattered contrasting during SEM of the coating as well as TNM substrate after isothermal exposure at 850 °C in ambient air for 100, 300, 600, and 1000 h are summarized in Fig. 3. Already after 100 h a dense TGO can be identified on top of the coating, see Fig. 3a.

The voids slightly below the TGO originate from Al diffusion to the surface to support the formation of Al_2O_3. This results in weakly bonded Ti enriched areas (partly due to or during the early stages of Kirkendall void formation), which break out during the metallographic preparation procedure. In the upper region of the coating, dark appearing precipitates formed in the otherwise bright appearing matrix, see also Fig. 3a. In the interface-near region, a homogenization zone formed by cross-diffusion between coating and TNM-alloy, causing also a change of the typical TNM microstructure due to the Al-enrichment. But about 10 µm further down into the TNM alloy its original microstructure (slightly refined) is still present. Increasing the exposure time to 300 h increases the TGO thickness, accompanied by a more pronounced void formation, see Fig. 3b. The dark appearing precipitates seem to be dissolved within the homogenization zones between coating and TNM alloy. The fined grained TNM microstructure underneath widens, which is related to the pronounced Al diffusion. Increasing the exposure times to 600 h intensifies these effects, but the TGO only slightly thickens, see Fig. 3c. Furthermore, the width of the homogenization zone stays quite constant, just the area of microstructural changes of the TNM alloy widens to 30 µm. After an exposure time of 1000 h (Fig. 3d), the still compact Al_2O_3-based TGO suggests that it is still supplied by sufficient Al through the internal Al-reservoir, and only slightly thicker than after 600 h. The progressing microstructural change of the TNM alloy is the major difference. Thus, the 16.5-µm-thick Al-rich γ-TiAl-based coating effectively protects the TNM alloy during exposure in ambient air at 850 °C for at least 1000 h.

The growth of the protective surface oxide, especially the oxygen inward diffusion as well as interdiffusion between coating and substrate, and their variation with time, is summarized in Fig. 4. The corresponding Ti, Al, and O concentration is depicted over depth after 100, 600, and 1000 h evaluated by SEM-EDS. Initial coating and TNM substrate material compositions are indicated by horizontal lines in Figs. 4a and 4b. These analyses show, that the oxide scale formation as well as interdiffusion between coating and TNM alloy, both driven by aluminum diffusion, take place simultaneously. After 100 h the titanium and aluminum content (green lines in Fig. 4a and b) basically decreased by the interdiffusion between coating and TNM alloy, forming the homogenization zone. In the surface-near region, about 4 at% Al was consumed from the coating to form a dense α-Al_2O_3-based TGO with a thickness of 1.5 µm. The dark grains within the top area of the coating (see Fig. 3a) are only present in an area where the Al content is close to the as-deposited state. We need to mention that around 5 at% oxygen stem from the sample preparation and thus build the background-level of the oxygen signal in Fig. 4c. The oxygen background level is due to surface oxidation between sample preparation and EDS investigation. The intersection between decreasing oxygen content (Fig. 4c) and increasing aluminum content (Fig. 4b) indicates the interface region between the formed TGO and the γ-TiAl-based coating. After 600 h oxidation at 850 °C, the Ti content within the coating increased to about 38 at% and its Al content decreased to about 51 at% in the vicinity of the TNM alloy. The latter shows a similar composition close to the coating, due to cross-diffusion, see Fig. 4b. The TGO just slightly thickened to 2.3 µm when exposed for 600 h at 850 °C (1.5 µm during the first 100 h) proving the outstanding ability of the Al-rich γ-TiAl-based coating to form a dense and protective α-Al_2O_3-based scale. Prolonging the exposure time to 1000 h causes no significant changes in the Al and Ti

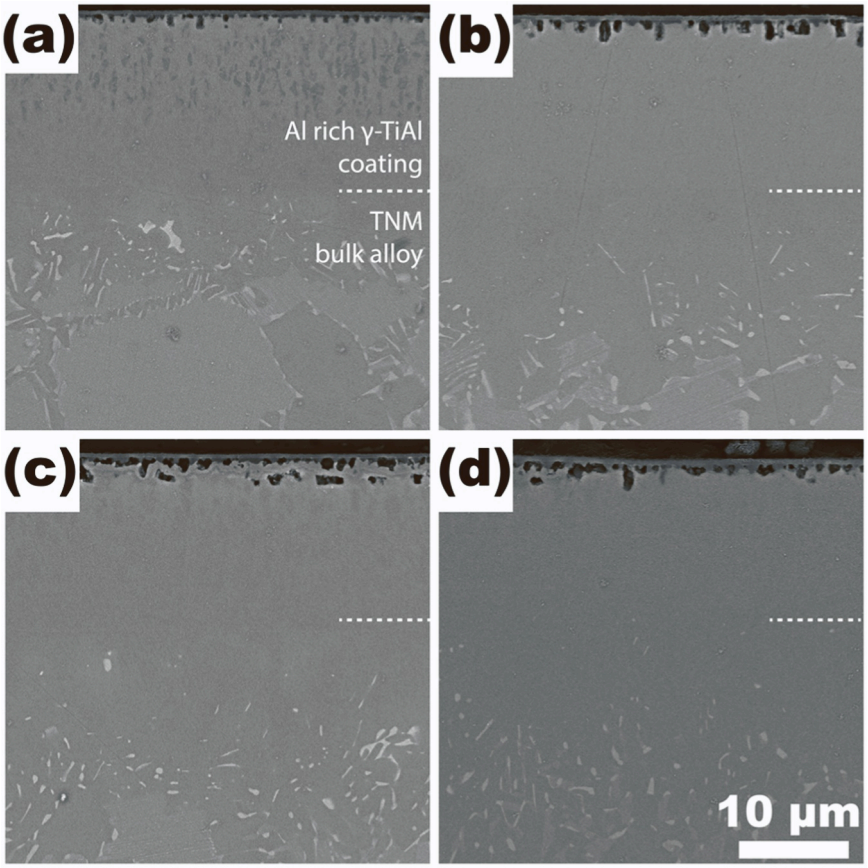

Fig. 3. Cross-sectional BSE-SEM images of coating-TNM alloy composites after oxidation at 850 °C in ambient air for 100 h (a), 300 h (b), 600 h (c), and 1000 h (d).

content. However, after 1000 h the Al content within the TGO is not 40 at% anymore (Al_2O_3 has 40 at% Al), indicating the additional formation of a very thin TiO_2 layer, also indicated by the Ti signal, see Fig. 4a. Nevertheless, the TGO is only about 3 µm thick after 1000 h oxidation at 850 °C, confirming its dense and protective nature.

Additional TEM as well as t-EBSD analysis of samples oxidized for 100, 600, and 1000 h allowed for even more detailed investigations on the ongoing microstructural and chemical changes. After 100 h in ambient air, the microstructure of the γ-TiAl-based coating clearly transformed from the original fibrous growth morphology towards a more equiaxed grain structure – compare Figs. 2a and 5a. This transformation process indicates that recrystallization proceeded, due to the relatively high temperature of about $0.5 \bullet T_m$ (T_m = 1733 K). The thermally grown oxide can clearly be identified at the very top of the coating, see Fig. 5b, having a very dense morphology. No obvious failure between TGO and γ-TiAl-based coating can be identified, which indicates an excellent adhesion. The voids directly underneath the TGO could partly stem from Kirkendall void formation (Al is needed for the TGO formation), as their surrounding is rich in Ti, see also inset 1 and the corresponding chemical map of Fig. 5. A more detailed phase analysis of the different predominant morphologies, darker and fine-grained areas as well as bright appearing zones in Fig. 5a, lead to the following conclusion. The more fine-grained morphology, as referred to the SAED indicated with 2, corresponds to γ-TiAl, the bright and large grains – see inset 3 in Fig. 5b – refer to Al-rich $TiAl_3$ domains. In more detail, this SAED from the coarser grains suggests the co-existence of $TiAl_3$ and γ-TiAl-based domains, whereas the globular grains can be assigned to the $TiAl_3$ phase and the fined grained surrounding to γ-TiAl. This stays in great agreement with the calculated phase diagram Ti-Al-4Nb-1-Mo, see Fig. S1 of the Appendix, specifically for the composition close to the TNM alloy. Additionally, t-EBSD investigations confirm the presence of $TiAl_3$ grains between the nanocrystalline γ-TiAl microstructure (Fig. 5c). The average size of these $TiAl_3$ grains is in the range of a few µm, with slightly smaller grains in the interface-near region close to the TNM alloy. The high Al content of 63 at% seems to be thermally stable over a wide exposure time of more than 100 h at 850 °C in ambient air. Furthermore, this Al-rich grains are also visible as dark gray domains in Fig. 3a.

The ongoing thermal exposure leads to a continuous Al diffusion, shifting the stable phase field from the Al-rich $TiAl_3$ and γ-TiAl domains to a single phased, γ-TiAl dominated microstructure. The consumption of Al-rich grains and growth of γ-TiAl-based domains is recognizable in Fig. 6a. Ageing up to 600 h leads again to a fine morphology of γ-TiAl-based grains, clearly visible in the TEM bright field image. Continuous Al-diffusion leads to a slight enlargement of the Kirkendall voids next to the TGO as well as the substrate coating interface. Focusing on the TGO, Fig. 6b shows a fine layer in between of two larger Al_2O_3-layers (indicated by SAED, inset 2 and also by EDS mapping, see inset 1. This fine layer originates due to TiN formation, which seems plausible through the absence of oxygen and the presence of Ti. A detailed consideration of the void affected region next to the interface, Fig. 6c, still proves a well adhering coating on the TNM substrate. The chemical mapping presented in inset 4 highlights the chemical balance in the interface-near region, which also proves the transition from the Al-rich $TiAl_3$ and γ-TiAl domains (overall 63 at% Al) to the γ-TiAl-phase field (50 at%) and hence nearly the same Al and Ti amount on both sides of the interface. This is also in perfect agreement with the SEM line scans presented in Fig. 4.

After 1000 h at 850 °C the coating morphology is characterized by larger grains at the top and smaller ones close to the substrate interface, see Fig. 7. The surface-near region (see Fig. 7b) was investigated in detail by high-resolution TEM and elemental mapping (inset 1 in Fig. 7b). This

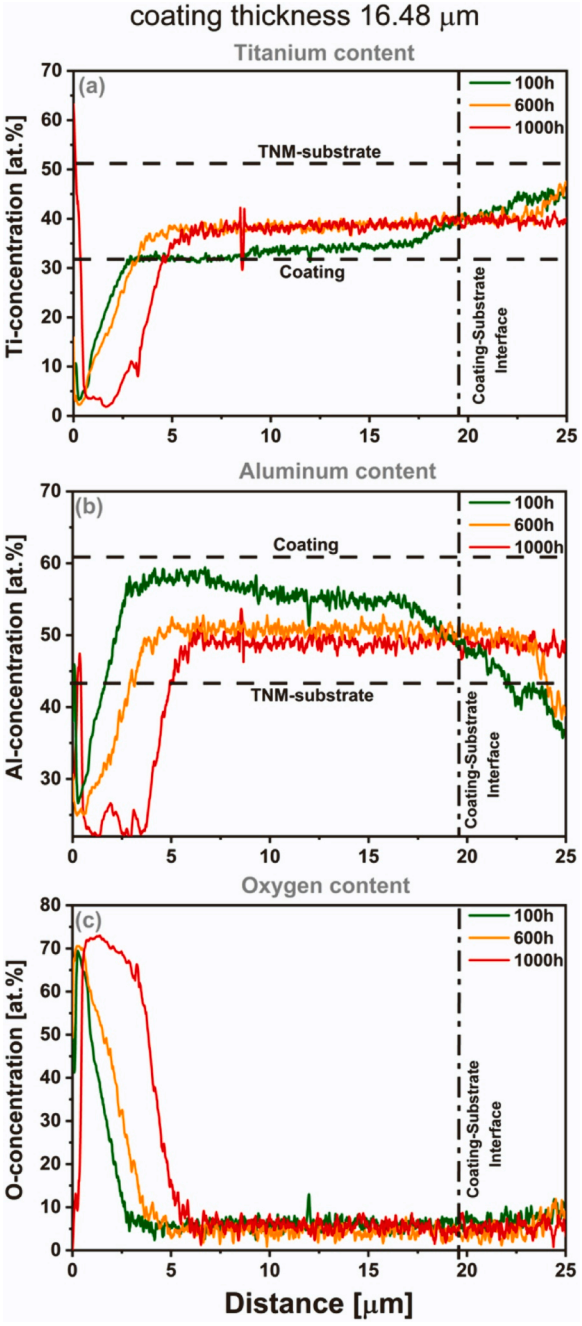

Fig. 4. Cross-sectional SEM-EDS line scans of coating-TNM alloy composites after oxidation at 850 °C in ambient air for 100, 600, and 1000 h. The Ti, Al, and O profile is given in (a), (b), and (c), respectively. The coating-TNM alloy interface is indicated by a vertical line, and the original Al and Ti contents of the coating (~62 at% Al and 32.7 at% Ti) and TNM alloy (~43.5 at% Al and 51.4 at% Ti) are indicated by horizontal lines. Especially, within the coarser grained substrate (with respect to the coating), the EDS signal is influenced by the different Al-contents of the individual phases, α, β, and/or γ, see the phase diagram, Fig. S1. Therefore, the Al-signal can (locally) be below the average original substrate value, like indicated by the signal close to 25 µm distance from the surface, obtained after 600 and 1000 h exposure.

investigation clearly shows that the TGO now also contains Ti, and at the boundary to the γ-TiAl-based coating also nitrogen. SAED analysis confirms the presence of TiO_2 within the TGO and TiN at the boundary to the γ-TiAl-based coating (not shown here). The overall slightly porous nature of the TGO, Fig. 7b, is a result of the TiO_2 formation. The mean grain size in the γ-TiAl-based coating below the TGO is about 1 µm, continuously decreasing to about 500 nm towards the TNM alloy, as studied by t-EBSD (see Fig. 7c). The Al content drops down to 50 at% and is now located in the stable γ-TiAl single phase field, as indicated in the calculated phase diagram, see Fig. S1 of the Appendix. Additionally, the t-EBSD investigation, Fig. 7c, shows only rarely dispersed a thin seam of Al-rich phases (i.e., $TiAl_2$ or $TiAl_3$), which surrounds the globular γ-TiAl grains. The Al-rich areas still decrease by diffusion and cannot hinder the further growth of γ-TiAl grains. The TNM alloy itself has a much larger grain size close to this interface, but compared to its original microstructure the grain size is also significantly reduced. The TEM-EDS line scan across the coating-TNM alloy interface shows a constant Al-content of 50 at% and no indication of oxygen or nitrogen (inset of Fig. 7c). This clearly highlights the excellent intermixing between γ-TiAl-based coating and TNM substrate (being essential for excellent adhesion) as well as the outstanding protective nature of the Al-rich γ-TiAl-based coating itself. The individual thicknesses of the TGO, Al-rich zone, and Al-depleted zone formed during the exposure times are summarized in Table 1.

Furthermore, detailed cross-sectional phase analysis was conducted by high-resolution X-ray nanodiffraction. Fig. 8a shows the thereby obtained intensity plot for the sample oxidized for 100 h at 850 °C. As indicated in Fig. 8a, the microstructure contains the full range of Al-rich phases (i.e., $TiAl_3$, Ti_2Al_5, Ti_5Al_{11}, or $TiAl_2$) down to γ-TiAl-based phases, whereas a clear separation is not trivial. This more or less multi-phased state is in agreement with the microstructure observed in Fig. 5, containing a mixture of globular Al-rich $TiAl_3$ domains next to fine-grained γ-TiAl. However, after 100 h oxidation, the remaining $TiAl_3$ can be recognized in the entire coating cross section.

Treating the sample for 1000 h at 850 °C further reduces the Al content close to the TNM alloy to 50 at% (see also Fig. 4). Thus, only directly beneath the TGO a sufficient Al-reservoir is still present, containing different Al-rich domains and corresponding phases, see Fig. 8b. Due to the cross-diffusion between coating and TNM alloy, which results in identical chemical composition across the initial coating–substrate interface, the nanodiffraction yields an identical phase composition for this region, being dominated by γ-TiAl.

A concluding scheme of the phase evolution process during oxidation is given in Fig. 9. According to equilibrium phase states, the as-deposited coating would be located with 63 at% Al in the γ-TiAl+$TiAl_3$-phase field, see also the calculated phase diagram, Fig. S1 of the Appendix. Based on the non-equilibrium nature of the physical vapor deposition process, the as-deposited coating exhibits off-stoichiometric phases, especially Al-rich ones (i.e., $TiAl_3$, Ti_2Al_5, Ti_5Al_{11}, or $TiAl_2$). After 100 h at 850 °C the Al-content stays constant, whereas the thermodynamically stable $TiAl_3$ grains clear growth, surrounded by fine crystalline γ-TiAl grains. Increasing the exposure time to 600 h results in a continuous Al-depletion, leading to a shift of the predominant phases from a mixture of Al-rich $TiAl_3$ domains accompanied by γ-TiAl, to a solely γ-TiAl dominated microstructure. Overcoming the recrystallization temperature in combination with the Al-depletion causes dissolution of the $TiAl_3$ phase and grain-growth of small γ-TiAl grains resulting in an additional fine-grained microstructure. Continuous annealing for 1000 h at 850 °C promotes grain-growth of γ-TiAl, exhibiting the well-known globular γ-TiAl grains, still surrounded by some residual Al-rich $TiAl_3$-seam. The Al depletion in the TNM substrate increases with time to a depth of approximately 30 µm and the TGO still exhibits a dense morphology (only slightly thickened to 2–3 µm) providing a stable, protective oxide layer. However, after 1000 h, a small amount of TiO_2 and TiN phases is detectable in the oxide-near region. The blocking of oxygen inward-diffusion to the TNM substrate (which would lead to embrittlement) was successfully obtained by stabilizing a dense and thermodynamically stable γ-TiAl zone, having a very low solubility for oxygen and hence preventing further inward-diffusion.

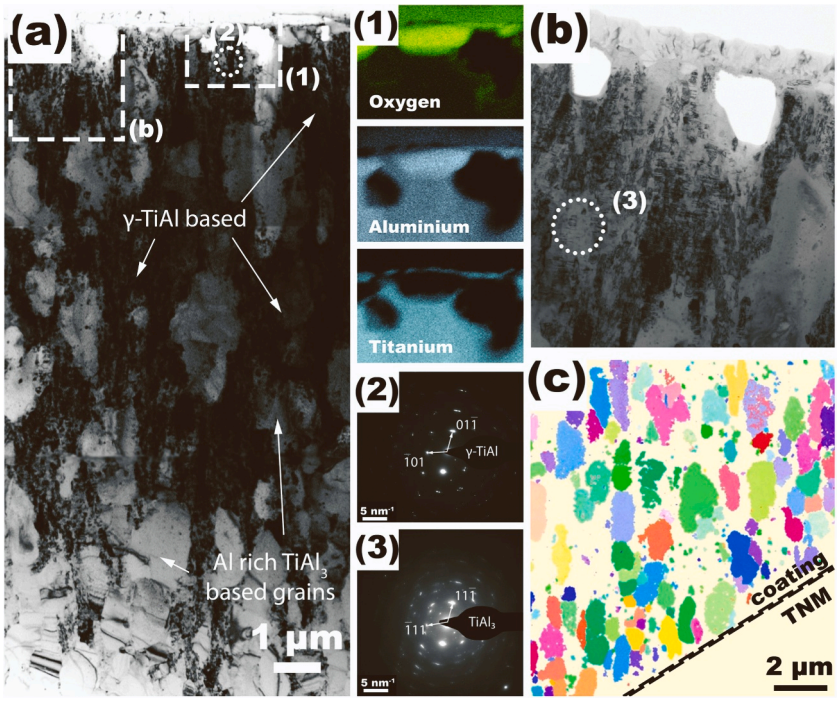

Fig. 5. Cross sectional TEM bright field image of the γ-TiAl-based coating after oxidation at 850 °C in ambient air for 100 h (a). Inset 1 presents the elemental map of region 1 indicated in (a), which exhibits the presence of an Al_2O_3 top-layer. In insets 2 and 3 the different morphological contributions are marked – small dark appearing fine grains correspond to γ-TiAl, while the large and bright appearing grains correspond to Al-rich $TiAl_3$ domains, see also (b). The t-EBSD image of the corresponding region is presented in (c), with red, green, and blue referring to 001-, 101-, and 111-orientations, respectively.

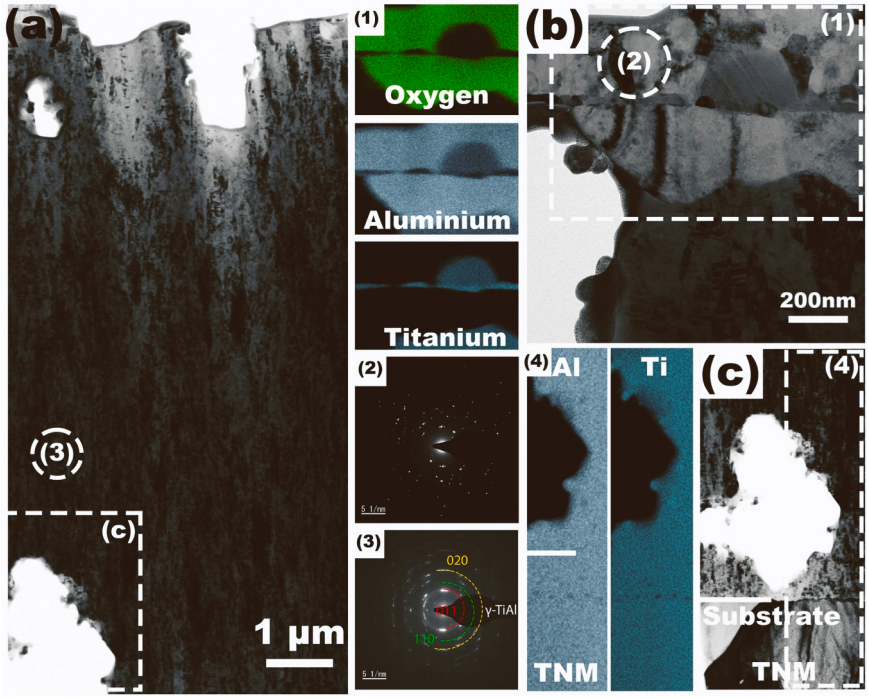

Fig. 6. Cross sectional TEM bright field image of the γ-TiAl-based coating after oxidation at 850 °C in ambient air for 600 h (a). This shows a fined grained γ-TiAl phase (see the respective SAED pattern of γ-TiAl, inset (3), whereas the coarse $TiAl_3$ grains are not present anymore and supposedly transformed to γ-TiAl. A higher magnification of the thermally grown oxide is given in (b). Inset 1 presents the elemental map of this region. The SAED of region (2) – within the dense, thermally grown oxide, see (b), where oxygen and aluminum is high, inset (1) – indicates α-Al_2O_3, inset (2). The dome-shaped region nearby, where the oxygen content is low, but the nitrogen content is high, see inset (1), is a TiN precipitate. (c) Kirkendall voids, filled with a sponge titanium network before preparation, appearing next to the interface. The representative EDS-mapping in inset 4 shows an equal Al and Ti content in the homogenization zone (the former interface is marked with a line).

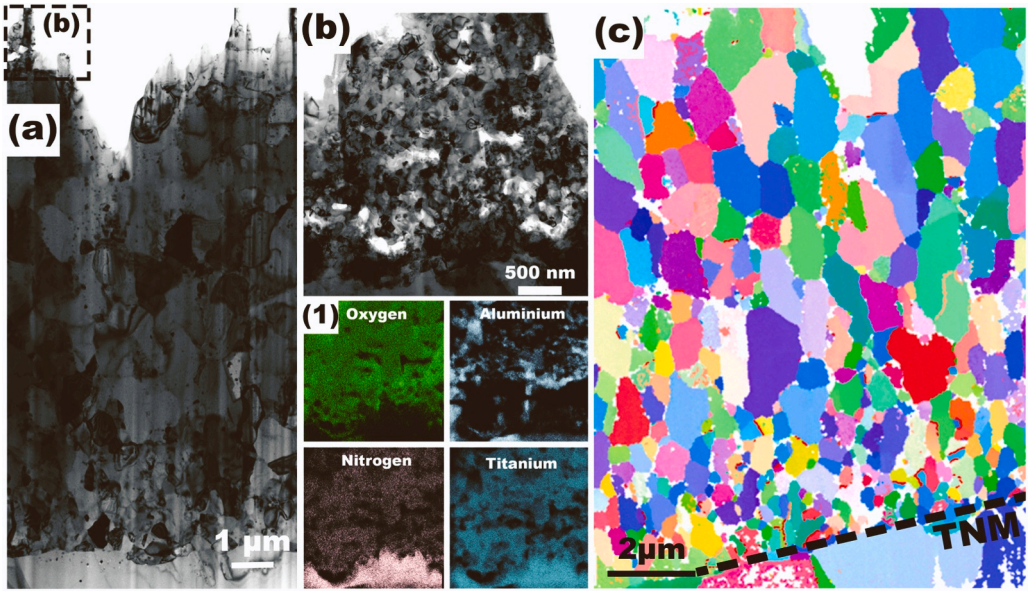

Fig. 7. Cross sectional TEM bright field image of the coating after oxidation at 850 °C in ambient air for 1000 h (a). A higher magnification of the top-most coating region is given in (b). Inset 1 presents the elemental map of this region. (c) t-EBSD image across the interface to the TNM alloy, with red, green, and blue referring to 001-, 100-, and 110-orientations, respectively. Due to aluminum loss, the γ-single phase field is reached, and EBSD, see (c), shows a coarse γ-grain structure.

Table 1
Thickness of the TGO, the Al-rich zone (III), and the Al-depletion zone (I) due to the thermal exposure at 850 °C for 100, 300, 600, and 1000 h of the coating. The original Al-rich γ-TiAl-based coating always had a thickness of 16.5 µm (for each treatment a fresh sample was used).

exposure time (h)	TGO (µm)	Al-rich zone III (µm)	Al-depletion zone I (µm)
100	1.30	7.61	0.84
300	2.12	15.25	1.93
600	2.85	13.32	2.52
1000	4.50	19.52	2.31

4. Conclusions

Increasing oxidation resistance of common TNM alloys gained a lot of attention in industry as well as academia. Especially, the field of thin protective films allows for excellent protection in hot oxidizing environment without influencing the mechanical properties of structural components. However, the fundamental issue of ceramic-like coatings is the (limited) adhesion to metallic substrate materials. Therefore, we deposited an Al-rich γ-TiAl-based coating – the dominating phases in as-deposited condition are γ-TiAl next to Al-rich TiAl phases $TiAl_2$, $TiAl_3$, Ti_2Al_5, and Ti_5Al_{11} – onto the TNM alloy. A short exposure to 850 °C leads to a $TiAl_3$ phase transformation between remaining TiAl, close to equilibrium phase contents. This transformation is influenced when Al depletes by outward diffusion to build a protective α-Al_2O_3-based oxide layer and (Ti and Al) cross-diffusion with the TNM substrate. The similarities in chemistry and structure between coating and TNM substrate allow for an outstanding adhesion – which further improves during thermal exposure through cross-diffusion (especially by Al) – and the high Al content (~62 at%) of the coating ensures an excellent oxidation resistance.

The high and sufficient Al-reservoir can be guaranteed at least up to

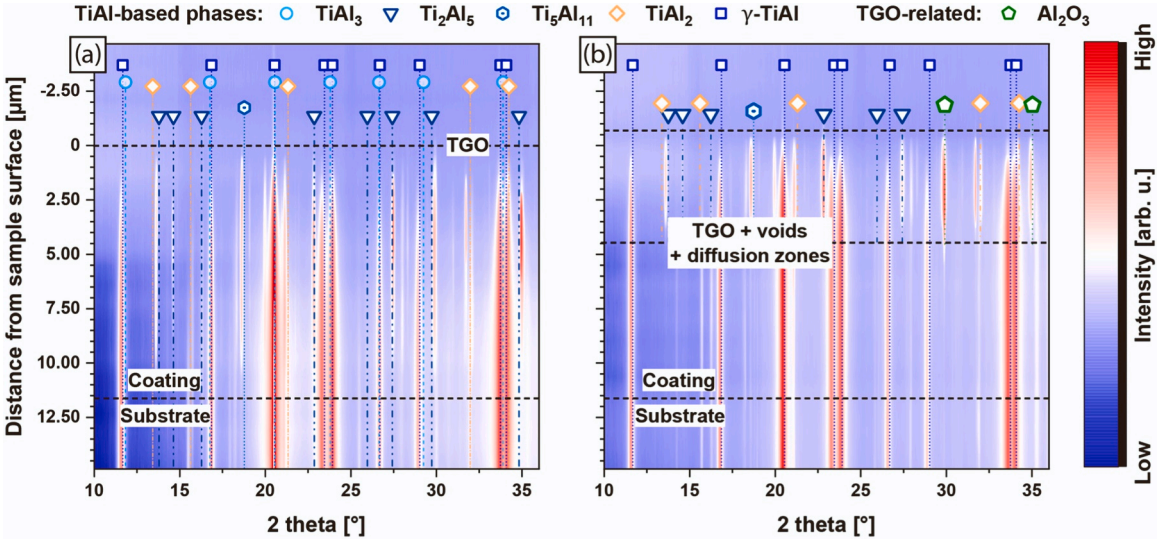

Fig. 8. Intensity vs. 2Θ dependence of the integrated patterns (full integrated) from nano beam experiments across the coating-TNM alloy interface for samples oxidized at 850 °C in ambient air for 100 h (a) and 1000 h (b).

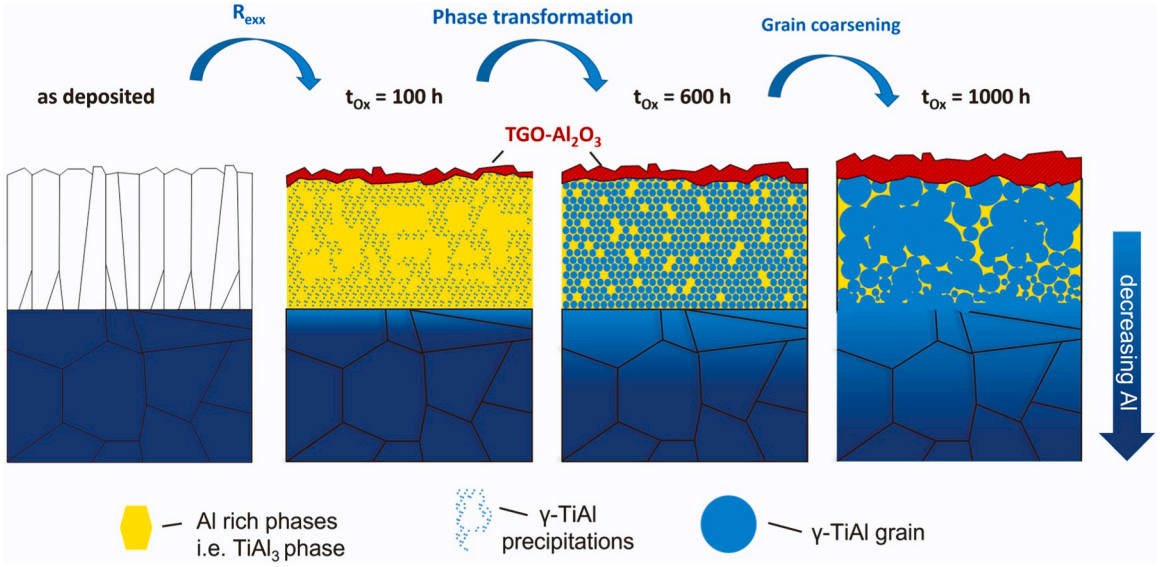

Fig. 9. Schematic evolution of the microstructure from the as-deposited state to an equilibrium state after 1000 h at 850 °C, due to the different phase transformations, which are forced by a continuous decreasing Al content caused by the TGO formation and coating/substrate homogenization inward diffusion.

1000 h at 850 °C in ambient air (max. combination tested here) for a 16.5-µm-thick coating, which allows the continuous formation of a dense and protective α-Al_2O_3-based thermally grown oxide. This TGO also shows an excellent bonding with the γ-TiAl-based coating and already after 100 h at 850 °C no interface between γ-TiAl-based coating and TNM substrate can be detected anymore. The so-called homogenization zone – same chemistry and microstructure as obtained by SEM, EDS-SEM, and nanodiffraction – widens with increasing annealing time and reaches about 30 µm after 1000 h. In the course of isothermal oxidation, the fine-fibrous growth morphology of the coating transforms into a different, more equiaxed morphology (from the TiAl/$TiAl_3$ two-phase field to the single TiAl phase field to a globular γ-TiAl structure) through recrystallization and phase transitions triggered by the continuous Al reduction in the coating. Especially, directly beneath the TGO, the high Al-reservoir can be sustained at least up to 1000 h (at 850 °C), after which the Al-rich $TiAl_3$ phases can still be detected by nanodiffraction – next to the dominating γ-TiAl. Al-reduction by (Al and Ti) cross-diffusion with the TNM substrate is faster than Al-reduction by outward diffusion to support the α-Al_2O_3-based oxide growth.

Based on the results presented, we can conclude that the ~62 at% Al containing γ-TiAl-based PVD coating (sputtered from a TiAl-GD7100 target, with 62 at%. Al) allows an excellent metallurgical bond with the TNM alloy (43.5 at% Al) and a significant improvement of its oxidation resistance, without any undesired phase formation and precipitation within the TNM alloy even during a 1000 h treatment at 850 °C.

CRediT authorship contribution statement

Stefan Kagerer: Investigation, Data curation, Writing – original draft. **Oliver E. Hudak:** Data curation. **Thomasz Wojcik:** Investigation, Visualization. **Rainer Hahn:** Investigation, Visualization. **Anton Davydok:** Investigation, Validation. **Martin Schloffer:** Conceptualization, Methodology. **Helmut Riedl:** Conceptualization, Methodology, Supervision, Project administration. **Paul H. Mayrhofer:** Conceptualization, Methodology, Resources, Writing – review & editing, Supervision, Project administration, Funding acquisition.

Declaration of Competing Interest

The authors declare that they have no known competing financial interests or personal relationships that could have appeared to influence the work reported in this paper.

Data Availability

Data will be made available on request.

Acknowledgements

The authors gratefully acknowledge the funding of the Federal Ministry for Economic Affairs and Climate Action of Germany (LuFo InnoMat Project: 20T1712). In addition, we also want to thank the X-ray center (XRC) of TU Wien for beam time as well as the electron microscopy center – USTEM TU Wien – for using the SEM facilities. The financial support by the Austrian Federal Ministry for Digital and Economic Affairs, the National Foundation for Research, Technology and Development and the Christian Doppler Research Association is gratefully acknowledged (Christian Doppler Laboratory "Surface Engineering of high-performance Components"). We further acknowledge the granted use of the Nanofocus Endstation of the Beamline P03 of PETRAIII at DESY, a member of the Helmholtz Association (HGF). The authors acknowledge TU Wien Bibliothek for financial support through its Open Access Funding Program.

Appendix A. Supporting information

Supplementary data associated with this article can be found in the online version at doi:10.1016/j.jallcom.2023.172343.

References

[1] J.P. Immarigeon, R.T. Holt, A.K. Koul, L. Zhao, W. Wallace, J.C. Beddoes, Lightweight materials for aircraft applications, Mater. Charact. 35 (1995) 41–67, https://doi.org/10.1016/1044-5803(95)00066-6.
[2] H. Clemens, W. Smarsly, Light-weight intermetallic titanium aluminides – status of research and development, Adv. Mater. Res. 278 (2011) 551–556, https://doi.org/10.4028/www.scientific.net/AMR.278.551.
[3] B.P. Bewlay, S. Nag, A. Suzuki, M.J. Weimer, TiAl alloys in commercial aircraft engines, Mater. High Temp. 33 (2016) 549–559, https://doi.org/10.1080/09603409.2016.1183068.
[4] M.C. Galetz, A.S. Ulrich, C. Oskay, D. Fähsing, N. Laska, U. Schulz, M. Schütze, Oxidation-induced microstructural changes of the TiAl TNM-B1 alloy after exposure at 900 °C in air, Intermetallics 123 (2020), https://doi.org/10.1016/j.intermet.2020.106830.

[5] A.M. Smyslov, A.A. Bybin, S.S. Dautov, Features of intermetallic alloy TNM-B1 high-temperature oxidation, Met. Sci. Heat. Treat. 58 (2016) 268–272, https://doi.org/10.1007/s11041-016-0001-0.
[6] A. Donchev, R. Pflumm, M. Galetz, S. Mayer, H. Clemens, M. Schutze, Oxidation protection of multiphase Mo-containing γ-TiAl-based alloys under cyclic test conditions, Mater. Res. Soc. Symp. . Proc. 1760 (2015) 205–210, https://doi.org/10.1557/opl.2015.160.
[7] W. Wallgram, T. Schmölzer, L. Cha, G. Das, V. Güther, H. Clemens, Technology and mechanical properties of advanced γ-TiAl based alloys, (n.d.) 1021–1030.
[8] A. Donchev, M. Schütze, Improving the oxidation resistance of γ-titanium aluminides by halogen treatment, Mater. Corros. 59 (2008) 489–493, https://doi.org/10.1002/maco.200804132.
[9] S. Friedle, R. Pflumm, A. Seyeux, P. Marcus, M. Schütze, ToF-SIMS Study on the Initial Stages of the Halogen Effect in the Oxidation of TiAl Alloys, Oxid. Met. 89 (2018) 123–139, https://doi.org/10.1007/s11085-017-9779-4.
[10] S. Friedle, N. Nießen, R. Braun, M. Schütze, Thermal barrier coatings on γ-TiAl protected by the halogen effect, Surf. Coat. Technol. 212 (2012) 72–78, https://doi.org/10.1016/j.surfcoat.2012.09.021.
[11] S. Kagerer, O.E. Hudak, M. Schloffer, H. Riedl, P.H. Mayrhofer, TGO formation and oxygen diffusion in Al-rich gamma-TiAl PVD-coatings on TNM alloys, Scr. Mater. 210 (2022), 114455, https://doi.org/10.1016/j.scriptamat.2021.114455.
[12] R. Braun, C. Leyens, M. Fröhlich, Performance of thermal barrier coatings on γ-TiAl, Mater. Corros. 56 (2005) 930–936, https://doi.org/10.1002/maco.200503925.
[13] R. Pflumm, S. Friedle, M. Schütze, Oxidation protection of γ-TiAl-based alloys - A review, Intermetallics 56 (2015) 1–14, https://doi.org/10.1016/j.intermet.2014.08.002.
[14] J. Małecka, Effect of an Al 2O 3 coating on the oxidation process of a γ-TiAl phase based alloy, Corros. Sci. 63 (2012) 287–292, https://doi.org/10.1016/j.corsci.2012.06.009.
[15] R. Braun, U. Schulz, C. Leyens, P.E. Hovsepian, A.P. Ehiasarian, Oxidation and fatigue behaviour of γ -TiAl coated with HIPIMS CrAlYN / CrN nanoscale multilayer coatings and EB-PVD thermal barrier coatings, 101, 2010.
[16] H. Asanuma, F.F. Klimashin, P. Polcik, S. Kolozsvári, H. Riedl, P.H. Mayrhofer, Impact of lanthanum and boron on the growth, thermomechanical properties and oxidation resistance of Ti–Al–N thin films, Thin Solid Films 688 (2019), 137239, https://doi.org/10.1016/j.tsf.2019.04.014.
[17] J.D. Béguin, J. Alexis, D. Adian, S. Metayer, T. Masri, J.A. Petit, P. Belaygue, MCrAlY Coatings for the Protection of Gamma Titanium Aluminide, Ti-2003 Science and Technology, Volume I: Proceedings of the 10th World Conference on Titanium Held at the CCH-Congress Center Hamburg, Germany July 13–18, 2003. 1, 2004, pp. 2455–2462.
[18] R. Braun, K. Kelm, M. Fröhlich, C. Leyens, Oxidation resistance of γ-TiAl based alloy Ti-45Al-8Nb coated with intermetallic Ti-Al-Cr-Y layers and EB-PVD zirconia topcoats at 950°C in air, Surf. Coat. Technol. 222 (2013) 128–134, https://doi.org/10.1016/j.surfcoat.2013.02.014.
[19] R. Braun, M. Fröhlich, C. Leyens, Intermetallic Ti-Al-Cr based layers and zirconia topcoats deposited on gamma titanium aluminides for environmental protection, Adv. Mater. Res. 278 (2011) 497–502, https://doi.org/10.4028/www.scientific.net/AMR.278.497.
[20] N. Laska, R. Braun, S. Knittel, Oxidation behavior of protective Ti-Al-Cr based coatings applied on the γ-TiAl alloys Ti-48-2-2 and TNM-B1, Surf. Coat. Technol. 349 (2018) 347–356, https://doi.org/10.1016/j.surfcoat.2018.05.067.
[21] A. Ebach-Stahl, C. Eilers, N. Laska, R. Braun, Cyclic oxidation behaviour of the titanium alloys Ti-6242 and Ti-17 with Ti – Al – Cr – Y coatings at 600 and 700 ° C in air, Surf. Coat. Technol. 223 (2013) 24–31, https://doi.org/10.1016/j.surfcoat.2013.02.021.
[22] M. Schloffer, H. Warnecke, Pub. No.: US 2018/163291 A1, 2018.
[23] W. Smarsly, M. Schloffer, H. Clemens, S. Mayer, Patent No.: US10465264B2, 2019.
[24] L. Zauner, P. Ertelthaler, T. Wojcik, H. Bolvardi, S. Kolozsvári, P.H. Mayrhofer, H. Riedl, Reactive HiPIMS deposition of Ti-Al-N: Influence of the deposition parameters on the cubic to hexagonal phase transition, Surf. Coat. Technol. 382 (2020), 125007, https://doi.org/10.1016/j.surfcoat.2019.125007.
[25] C. Krywka, J. Keckes, S. Storm, A. Buffet, S.V. Roth, R. Döhrmann, M. Müller, Nanodiffraction at MINAXS (P03) beamline of PETRA III, J. Phys.: Conf. Ser. 425 (2013), https://doi.org/10.1088/1742-6596/425/7/072021.
[26] J. Keckes, M. Bartosik, R. Daniel, C. Mitterer, G. Maier, W. Ecker, J. Vila-Comamala, C. David, S. Schoeder, M. Burghammer, X-ray nanodiffraction reveals strain and microstructure evolution in nanocrystalline thin films, Scr. Mater. 67 (2012) 748–751, https://doi.org/10.1016/J.SCRIPTAMAT.2012.07.034.
[27] G. Benecke, W. Wagermaier, C. Li, M. Schwartzkopf, G. Flucke, R. Hoerth, I. Zizak, M. Burghammer, E. Metwalli, P. Müller-Buschbaum, M. Trebbin, S. Förster, O. Paris, S.V. Roth, P. Fratzl, A customizable software for fast reduction and analysis of large X-ray scattering data sets: applications of the new DPDAK package to small-angle X-ray scattering and grazing-incidence small-angle X-ray scattering, J. Appl. Crystallogr. 47 (2014) 1797–1803, https://doi.org/10.1107/S1600576714019773.